

Vox2Vox: 3D-GAN for Brain Tumour Segmentation

Marco Domenico Cirillo^{1,2}, David Abramian^{1,2}, and Anders Eklund^{1,2,3}

¹ Department of Biomedical Engineering

² Center for Medical Image Science and Visualization

³ Division of Statistics and Machine learning, Department of Computer and Information Science
Linköping University, Linköping, Sweden

Abstract. We propose a 3D volume-to-volume Generative Adversarial Network (GAN) for segmentation of brain tumours. The proposed model, called Vox2Vox, generates segmentations from multi-channel 3D MR images. The best results are obtained when the generator loss (a 3D U-Net) is weighted 5 times higher compared to the discriminator loss (a 3D GAN). For the BraTS 2018 training set we obtain (after ensembling 5 models) the following dice scores and Hausdorff 95 percentile distances: 90.66%, 82.54%, 78.71%, and 4.04 mm, 6.07 mm, 5.00 mm, for whole tumour, core tumour and enhancing tumour respectively. The proposed model is shown to compare favorably to the winners of the BraTS 2018 challenge, but a direct comparison is not possible.

Keywords: MRI · Vox2Vox · Generative Adversarial Networks · deep learning · artificial intelligence · 3D image segmentation.

1 Introduction

Gliomas are the most frequent intrinsic tumours of the central nervous system and encompass two principle subgroups: diffuse gliomas (high grade gliomas, HGG), and gliomas showing a more circumscribed growth pattern (low grade gliomas, LGG) [31]. Although both these brain tumours types can be detected, they have a diffuse, infiltrative way of growing in the brain, and they exhibit peritumoural oedema, such as an increase in water content in the area surrounding the tumour. This makes it arduous to define the tumour border by visual assessment, both in analysis and also during surgery [5].

For this reason, researchers started recently to resort to powerful techniques, able to segment complex objects and, in this way, guide the surgeons during the operation with a suitable accuracy. Indeed, machine learning [25] and deep learning [12,14,17,20,23,29] can provide state-of-the-art segmentation results.

1.1 Related Works

Nowadays generative adversarial networks (GANs) [9] are gaining popularity in computer vision, since they can learn to synthesise virtually any type of image.

Specifically, GANs can be used for style transfer [8], image synthesis from noise [15], image to image translation [13], and also image segmentation [27]. GANs have become especially popular in medical imaging [32] since medical imaging datasets are much smaller compared to general computer vision datasets such as ImageNet. Additionally, it is common to collect several image modalities for each subject before proceeding with the analysis, and, when this cannot be possible, CycleGAN introduced in [33] can be used to synthesize those missing modalities.

GANs have also been used for medical image segmentation. Indeed, Z. Han *et al.* in [10] proposed a GAN to segment multiple spinal structures in MRIs; Y. Li *et al.* in [19] developed a novel transfer-learning framework using a GAN for robust segmentation of different human epithelial type 2 (HEp-2) cells; X. Dong *et al.* in [6] implemented a U-Net style GAN for accurate and timely organs-at-risk (OARs) segmentation; S. Nema *et al.* in [24] designed a 2D GAN, called RescueNet, to segment brain tumours from MR images; etc. Yi *et al.* [32] provide a complete and recent review of GANs applied in medicine.

Hence, inspired by these works and especially by the Pix2Pix GAN [13], which can generate an image of type A from an image of type B, the aim of this project is to do 3D image segmentation using 3D Pix2Pix GAN, named Vox2Vox, to segment brain gliomas. While a normal convolutional neural network, such as U-Net [26], performs the segmentation pixel by pixel, or voxel by voxel, through maximizing a segmentation metric or metrics (i.e. dice score, intersection over union, etc), a GAN will also punish segmentation results that do not look realistic. Our hypothesis is that this can result in better segmentations.

2 Method

2.1 Data

The MR images used for this project are the Multimodal Brain tumour Segmentation Challenge (BraTS) 2018 training ones [1,2,3,4,21]. The BraTS 2018 training dataset contains MR volumes of shape $240 \times 240 \times 155$ from 285 patients, and for each patient four types of MR images were collected: native (T1), post-contrast T1-weighted (T1Gd), T2-weighted (T2), and T2 Fluid Attenuated Inversion Recovery (FLAIR). The data were acquired from 19 different institutions with different clinical protocols. The tumours have been segmented manually, by one to four raters, following the same annotation protocol, and their annotations were approved by experienced neuro-radiologists. Figure 1 shows an example of one of the test volumes.

2.2 Image Pre-processing

For each MR image intensity normalization is done per channel, whereas the background voxels are fixed to 0. On the other hand, the grey-scale ground-truths are transformed into categorical, so each target has four channels, as the number of the classes to segment: background, peritumoural edema (ED),

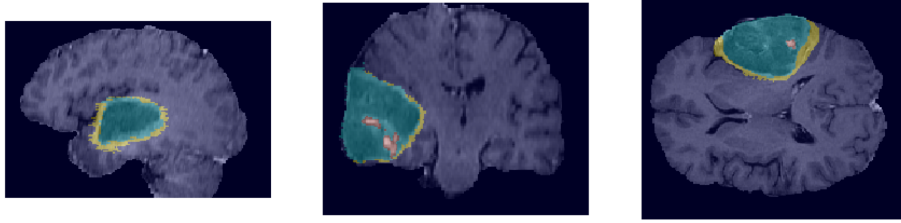


Fig. 1. From left to right there is a T1-weighted MR image in the sagittal, coronal and transverse plane overlapped with its ground-truth segmentations. Peritumoural edema (ED), necrotic and non-enhancing tumour core (NCR/NET), and GD-enhancing tumour (ET) are highlighted in yellow, cyan and red respectively.

necrotic and non-enhancing tumour core (NCR/NET), and GD-enhancing tumour (ET) labeled with 0, 1, 2, 3 respectively.

Since the BraTS volumes are memory demanding, patch augmentation is applied to extract one sub-volume of $128 \times 128 \times 128$ from each original volume. In this way, only 23.5% of the whole training set is used in every training epoch.

The training, validation and testing sets are split into 182 (64%), 46 (16%) and 57 (20%) volumes respectively.

2.3 Model Architecture

The Vox2Vox model, as the Pix2Pix one [13], consists of a generator and a discriminator. The generator, illustrated by Figure 2, is built as U-Net [26]:

- I*: a 3D image with 4 channels: T1, T2, T1Gd, and T2 FLAIR;
- E*: four 3D convolutions using kernel size $4 \times 4 \times 4$, stride 2 and same padding, followed by instance normalization [30] and Leaky ReLU activation function. The number of filters used at the first 3D convolution is 64 and at each down-sampling the number is doubled;
- B*: four 3D convolutions using kernel size $4 \times 4 \times 4$, stride 1 and same padding, followed by instance normalization and Leaky ReLU activation function. Every convolution-normalization-activation output is concatenated with the previous one;
- D*: three 3D transpose convolutions using kernel size $4 \times 4 \times 4$ and stride 2, followed by instance normalization and ReLU activation. Each 3D convolution input is concatenated with the respective encoder output layer;
- O*: segmentation prediction of size $128 \times 128 \times 128 \times 4$ given by a 3D transpose convolution using 4 filters (as the number of the classes to segment), kernel size $4 \times 4 \times 4$ and stride 2, followed by softmax activation function generates 4 channel segmentation prediction of the input image.

On the other hand, the discriminator consists of:

- I*: the 3D image with 4 channels and its segmentation ground-truth or the generator’s segmentation prediction;

E : the same of the generator;

O : volume of size $8 \times 8 \times 8 \times 1$ given by a 3D convolution using 1 filter, kernel size $4 \times 4 \times 4$, stride 1 and same padding generates the discriminator output, used to determine the quality of the segmentation prediction created by the generator.

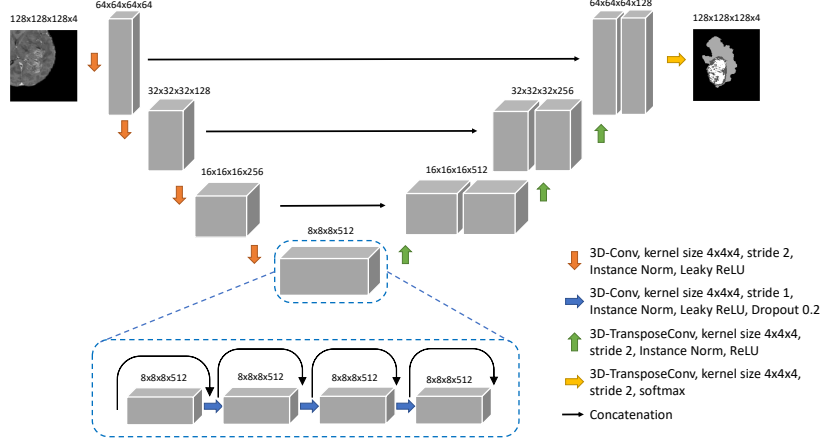


Fig. 2. The generator model with 3D U-Net architecture style.

All the kernel weights for each 3D convolution are initialized using the He *et al.* method [11] and all Leaky ReLU layers have slope coefficient 0.3. On the other hand, I , E , B , D , and O here stand for input(s), encoder, bottleneck, decoder, and output respectively.

2.4 Losses

Since Vox2Vox contains two models, the generator and the discriminator, two loss functions are used. The discriminator loss, L_D , is the sum between the L_2 error of the discriminator output, $D(\cdot, \cdot)$, between the original image x and the respective ground-truth y with a tensor of ones, and the L_2 error of the discriminator output between the original image and the respective segmentation prediction \hat{y} given by the generator with a tensor of zeros, i.e.:

$$L_D = L_2 [D(x, y), \mathbf{1}] + L_2 [D(x, \hat{y}), \mathbf{0}] , \quad (1)$$

whereas, the generator loss, L_G , is the sum between the L_2 error of the discriminator output between the original image and the respective segmentation prediction given by the generator with a tensor of ones, and the generalized dice loss [22,28], $GDL(\cdot, \cdot)$, between the ground-truth and the generator's output multiplied by the scalar $\alpha \geq 0$, i.e.:

$$L_G = L_2 [D(x, \hat{y}), \mathbf{1}] + \alpha GDL [y, \hat{y}] . \quad (2)$$

By looking at Equation 2, it is easy to conclude that if $\alpha = 0$: Vox2Vox is a pure GAN and it minimizes only the unsupervised loss given by the discriminator; whereas if $\alpha \rightarrow \infty$: Vox2Vox ignores the discriminator output, and so it behaves more as a 3D U-Net.

2.5 Optimization and Regularization

Both the generator and the discriminator are trained using the Adam optimizer [16] with the parameters: $\lambda = 2 \cdot 10^{-4}$, $\beta_1 = 0.5$, and $\beta_2 = 0.999$. Dropout regularization with a dropout probability of 0.2 is used after each 3D convolutional operation in the generator’s bottleneck (see Figure 2). Moreover, as X. Yi reported in [32], the discriminator loss helps the generator to guarantee the spatial consistency in the final results, behaving as a shape regularizer. In other words, the discriminator takes care that the generated brain segmentation looks realistic (i.e. like manual segmentations). In the end, we expect that Vox2Vox performs better with a trade-off α which does not disregard completely the discriminator loss and, at the same time, does not disregard the generator either.

2.6 Model Ensembling

Once the network is implemented, it is possible to do M -fold cross-validation and then ensemble all the models in order to have a more robust segmentation prediction [14]. The ensemble is simply done by averaging the class probabilities voxel-per-voxel, given by the softmax activation function, of the predictions produced by each cross-validation model, i.e.:

$$\hat{y}_E = P(y|x) = \frac{1}{M} \sum_{i=1}^M P(y|x, m_i), \quad (3)$$

where \hat{y}_E is the ensemble prediction of the target y given the MR images x , whereas $P(y|x, m_i)$, with $i = 1, \dots, M$ and M is the number of models to ensemble, is the prediction of the target y given the MR images x using the i -th model m .

3 Results

The Vox2Vox model is implemented using Python 3.7, Tensorflow 2.1 and its Keras library. The code is available on Github⁴.

The model is trained and validated on sub-volumes of size $128 \times 128 \times 128$ from 182 and 46 subjects respectively, using batch size 4, over 200 epochs on a computer equipped with 128 GB RAM and an Nvidia GeForce RTX 2080 Ti graphics card with 11 GB of memory. Once the training is completed, the 57 testing volumes are cropped in order to have shape $160 \times 192 \times 128$. In this

⁴ <https://github.com/mdciri/Vox2Vox>

way, the testing set can be given as input to the fully convolutional Vox2Vox, because each axis is now divisible by $2^4 = 16$, where 4 is the generator’s and discriminator’s depth.

After many attempts, we decided that a good trade-off to weight the discriminator and the generator is when $\alpha = 5$. Table 1 reports the dice and the Hausdorff distance 95 percentile scores between the ground-truth and the generated predictions over the testing set. Note that the tumour’s classes are reset as: whole tumour ($WT = ET \cup NCR/NET \cup ED$), tumour core ($TC = ET \cup NCR/NET$) and enhancing tumour (ET).

Table 1. Dice score and Hausdorff distance 95 percentile for the different brain tumour areas for the testing set. The metrics here are obtained when training the model with sub-volumes of $128 \times 128 \times 128$ voxels, $\alpha = 5$, and with image augmentation: random patch extraction (PE), flipping (F) and rotation (R).

Aug. tech.	Dice score [%]			Hausdorff distance 95 [mm]		
	WT	TC	ET	WT	TC	ET
PE	88.62	78.30	74.81	6.82	7.79	7.66
PE + F	88.76	78.78	73.82	8.19	9.34	8.75
PE + R	89.66	77.64	74.35	6.23	11.55	9.03
PE + F + R	89.73	81.02	77.46	4.60	6.97	5.00

Table 1 also reports the scores when applying random flipping, random rotations between 0° and 30° , or both in the three spatial axes as image augmentation. The best choice is to apply both flipping and rotation as image augmentation, because they increase substantially all the metrics for each class of interest. It takes between 8 and 9 minutes to complete one epoch when extracting batches from a Keras generator (reading volumes from the hard drive), or between 4 and 5 minutes if all training and validation sub-volumes are stored in CPU memory.

In the end, training and validation set are merged and then divided into 5 folds in order to perform 5-fold cross-validation on the Vox2Vox trained on sub-volumes of $128 \times 128 \times 128$ voxels, using $\alpha = 5$ and applying flipping and rotation as augmentation. Table 2 reports the scores obtained from such cross-validation and also those from the ensemble of these 5 models, as explained in Equation 3. Figure 3 shows an example of segmentation prediction realized by such ensembling.

It is interesting to notice in Table 2 that even if the fifth model behaves worse than the others, this does not severely affect the ensemble’s performance which is better than every single model’s one. Moreover, Table 2 also compares the

Table 2. Dice score and Hausdorff distance 95 percentile for the different brain tumour areas on the testing set. The metrics reported here are the average (avg) and standard deviation (std) for each class after 5-fold cross-validation (CV). These metrics are extracted after ensembling these 5 models trained on sub-volumes of $128 \times 128 \times 128$ voxels, using $\alpha = 5$ and applying both flip and rotation as image augmentation.

	Dice score [%]			Hausdorff distance 95 [mm]		
	WT	TC	ET	WT	TC	ET
model 1	89.73	81.02	77.46	4.60	6.97	5.00
model 2	90.19	81.64	77.89	4.38	5.95	5.00
model 3	89.42	78.37	75.01	5.26	8.49	7.07
model 4	90.34	80.07	77.62	7.37	7.73	6.07
model 5	86.57	70.69	72.78	5.51	10.52	6.48
CV avg	89.25	78.36	76.15	5.42	7.93	5.92
CV std	1.37	3.99	1.97	1.05	1.54	0.81
ensemble	90.66	82.54	78.71	4.04	6.07	5.00
A. Myronenko [23]	88.39	81.54	76.64	5.90	4.81	3.77
F. Isensee <i>et al.</i> [12]	87.81	80.62	77.88	6.03	5.08	2.90

obtained segmentation metrics with those reported in [12] and [23], winners of the 2nd and 1st BraTS challenge 2018 place respectively. Those results were obtained ensembling 10 and 2 models (ensembled by 5 other models each) respectively and training, validating and testing on 285 (our whole dataset), 66 and 191 3D MR images, so an exact comparison cannot be done. Anyway, ensembling 5 Vox2Vox models into 1 model returns a stronger network able to segment brain tumours with better dice scores, almost 1-2% better for each class, but worse Hausdorff distances for the core and enhancing tumour. We think that this might be due to shape regularization introduced by the discriminator.

4 Conclusion

Figure 3 and Table 2 establish that the ensemble of multiple Vox2Vox models return high quality segmentation outputs: achieving 90.66%, 82.54%, 78.71% dice, and 4.04mm, 6.07mm, 5.00mm Hausdorff distance 95 percentile scores for whole tumour, core tumour and enhancing tumour respectively. The values reported

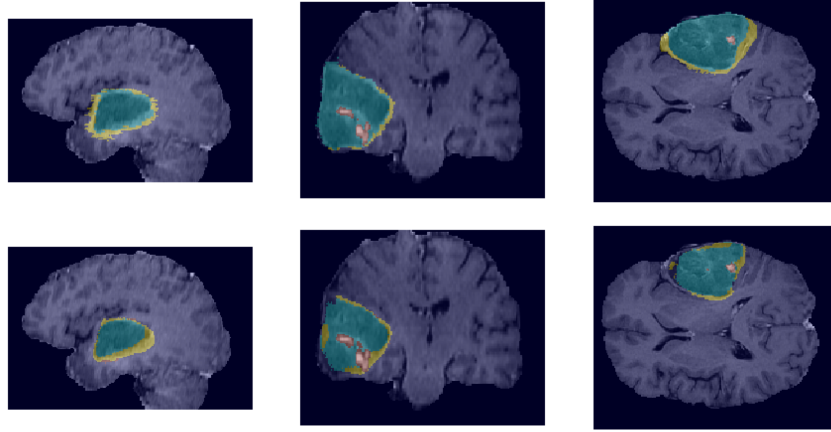


Fig. 3. Top: an example of a T1-weighted MR image in the sagittal, coronal and transverse plane overlapped with its ground-truth segmentation. Bottom: the predicted segmentation made by the ensemble model. Peritumoural edema (ED), necrotic and non-enhancing tumour core (NCR/NET), and GD-enhancing tumour (ET) are highlighted in yellow, cyan and red respectively.

are better than those of the first two winners of the BraTS 2018 challenge, but as previously explained a direct comparison is not possible.

These values compare favorably to the first two winners of the BraTS 2018 challenge, but at the same time those networks were trained and tested on more data than here and more models were used for the ensemble.

In the end, the Vox2Vox model can be used not only for image segmentation but also for further image augmentation. Indeed, Vox2Vox could be combined with a 3D noise to image GAN [7,18] which can synthesize realistic ground truth segmentations, that are then translated to realistic MR volumes. This combination might result in a fast batch generator of MR images, with ground-truth segmentations for training another network. It would be interesting to participate in the next BraTS challenge with the Vox2Vox model, in order to evaluate it with an ampler brain tumour image dataset than the one used here.

Acknowledgement

This study was supported by VINNOVA Analytic Imaging Diagnostics Arena (AIDA) and the ITEA3 / VINNOVA funded project Intelligence based iMprovement of Personalized treatment And Clinical workflow support (IMPACT). Funding was also provided by the Center for Industrial Information Technology (CENIIT) at Linköping University.

References

1. Bakas, S., Akbari, H., Sotiras, A., Bilello, M., Rozycki, M., Kirby, J., Freymann, J., Farahani, K., Davatzikos, C.: Segmentation labels and radiomic features for the pre-operative scans of the TCGA-GBM collection. The Cancer Imaging Archive (2017)
2. Bakas, S., Akbari, H., Sotiras, A., Bilello, M., Rozycki, M., Kirby, J., Freymann, J., Farahani, K., Davatzikos, C.: Segmentation labels and radiomic features for the pre-operative scans of the TCGA-LGG collection. The Cancer Imaging Archive **286** (2017)
3. Bakas, S., Akbari, H., Sotiras, A., Bilello, M., Rozycki, M., Kirby, J.S., Freymann, J.B., Farahani, K., Davatzikos, C.: Advancing the cancer genome atlas glioma MRI collections with expert segmentation labels and radiomic features. Scientific data **4**, 170117 (2017)
4. Bakas, S., Reyes, M., Jakab, A., Bauer, S., Rempfler, M., Crimi, A., Shinohara, R.T., Berger, C., Ha, S.M., Rozycki, M., et al.: Identifying the best machine learning algorithms for brain tumor segmentation, progression assessment, and overall survival prediction in the BRATS challenge. arXiv preprint arXiv:1811.02629 (2018)
5. Blystad, I.: Clinical Applications of Synthetic MRI of the Brain, vol. 1600. Linköping University Electronic Press (2017)
6. Dong, X., Lei, Y., Wang, T., Thomas, M., Tang, L., Curran, W.J., Liu, T., Yang, X.: Automatic multiorgan segmentation in thorax CT images using U-net-GAN. Medical physics **46**(5), 2157–2168 (2019)
7. Eklund, A.: Feeding the zombies: Synthesizing brain volumes using a 3D progressive growing GAN. arXiv:1912.05357 (2019)
8. Gatys, L.A., Ecker, A.S., Bethge, M.: Image style transfer using convolutional neural networks. In: Proceedings of the IEEE conference on computer vision and pattern recognition. pp. 2414–2423 (2016)
9. Goodfellow, I., Pouget-Abadie, J., Mirza, M., Xu, B., Warde-Farley, D., Ozair, S., Courville, A., Bengio, Y.: Generative adversarial nets. In: Advances in neural information processing systems. pp. 2672–2680 (2014)
10. Han, Z., Wei, B., Mercado, A., Leung, S., Li, S.: Spine-GAN: Semantic segmentation of multiple spinal structures. Medical image analysis **50**, 23–35 (2018)
11. He, K., Zhang, X., Ren, S., Sun, J.: Delving deep into rectifiers: Surpassing human-level performance on imagenet classification. In: Proceedings of the IEEE international conference on computer vision. pp. 1026–1034 (2015)
12. Isensee, F., Kickingereder, P., Wick, W., Bendszus, M., Maier-Hein, K.H.: No new-net. In: International MICCAI Brainlesion Workshop. pp. 234–244. Springer (2018)
13. Isola, P., Zhu, J.Y., Zhou, T., Efros, A.A.: Image-to-image translation with conditional adversarial networks. In: Proceedings of the IEEE conference on computer vision and pattern recognition. pp. 1125–1134 (2017)
14. Kamnitsas, K., Bai, W., Ferrante, E., McDonagh, S., Sinclair, M., Pawlowski, N., Rajchl, M., Lee, M., Kainz, B., Rueckert, D., et al.: Ensembles of multiple models and architectures for robust brain tumour segmentation. In: International MICCAI Brainlesion Workshop. pp. 450–462. Springer (2017)
15. Karras, T., Aila, T., Laine, S., Lehtinen, J.: Progressive growing of GANs for improved quality, stability, and variation. ICLR (2018)
16. Kingma, D.P., Ba, J.: Adam: A method for stochastic optimization. arXiv preprint arXiv:1412.6980 (2014)

17. Kong, X., Sun, G., Wu, Q., Liu, J., Lin, F.: Hybrid pyramid U-Net model for brain tumor segmentation. In: International Conference on Intelligent Information Processing. pp. 346–355. Springer (2018)
18. Kwon, G., Han, C., Kim, D.s.: Generation of 3D brain MRI using auto-encoding generative adversarial networks. In: International Conference on Medical Image Computing and Computer-Assisted Intervention. pp. 118–126 (2019)
19. Li, Y., Shen, L.: cC-GAN: A robust transfer-learning framework for HEP-2 specimen image segmentation. *IEEE Access* **6**, 14048–14058 (2018)
20. McKinley, R., Meier, R., Wiest, R.: Ensembles of densely-connected CNNs with label-uncertainty for brain tumor segmentation. In: International MICCAI Brainlesion Workshop. pp. 456–465. Springer (2018)
21. Menze, B.H., Jakab, A., Bauer, S., Kalpathy-Cramer, J., Farahani, K., Kirby, J., Burren, Y., Porz, N., Slotboom, J., Wiest, R., et al.: The multimodal brain tumor image segmentation benchmark (BRATS). *IEEE transactions on medical imaging* **34**(10), 1993–2024 (2014)
22. Milletari, F., Navab, N., Ahmadi, S.A.: V-net: Fully convolutional neural networks for volumetric medical image segmentation. In: 2016 Fourth International Conference on 3D Vision (3DV). pp. 565–571. IEEE (2016)
23. Myronenko, A.: 3D MRI brain tumor segmentation using autoencoder regularization. In: International MICCAI Brainlesion Workshop. pp. 311–320. Springer (2018)
24. Nema, S., Dudhane, A., Murala, S., Naidu, S.: RescueNet: An unpaired GAN for brain tumor segmentation. *Biomedical Signal Processing and Control* **55**, 101641 (2020)
25. Polly, F., Shil, S., Hossain, M., Ayman, A., Jang, Y.: Detection and classification of HGG and LGG brain tumor using machine learning. In: 2018 International Conference on Information Networking (ICOIN). pp. 813–817. IEEE (2018)
26. Ronneberger, O., Fischer, P., Brox, T.: U-net: Convolutional networks for biomedical image segmentation. In: International Conference on Medical image computing and computer-assisted intervention. pp. 234–241. Springer (2015)
27. Sato, M., Hotta, K., Imanishi, A., Matsuda, M., Terai, K.: Segmentation of Cell Membrane and Nucleus by Improving Pix2pix. In: BIOSIGNALS. pp. 216–220 (2018)
28. Sudre, C.H., Li, W., Vercauteren, T., Ourselin, S., Cardoso, M.J.: Generalised dice overlap as a deep learning loss function for highly unbalanced segmentations. In: Deep learning in medical image analysis and multimodal learning for clinical decision support, pp. 240–248. Springer (2017)
29. Topol, E.J.: High-performance medicine: the convergence of human and artificial intelligence. *Nature medicine* **25**(1), 44–56 (2019)
30. Ulyanov, D., Vedaldi, A., Lempitsky, V.: Instance normalization: The missing ingredient for fast stylization. *arXiv preprint arXiv:1607.08022* (2016)
31. Wesseling, P., Capper, D.: Who 2016 classification of gliomas. *Neuropathology and applied neurobiology* **44**(2), 139–150 (2018)
32. Yi, X., Walia, E., Babyn, P.: Generative adversarial network in medical imaging: A review. *Medical image analysis* p. 101552 (2019)
33. Zhu, J.Y., Park, T., Isola, P., Efros, A.A.: Unpaired image-to-image translation using cycle-consistent adversarial networks. In: Proceedings of the IEEE international conference on computer vision. pp. 2223–2232 (2017)